Assessing Cloud Structure Using Parametrized and Self-Consistent Models in Retrieval

Ashley D. Baker[1]
Project Mentor: Jasmina Blecic[2]
[1] *Physics & Astronomy Department, University of Pennsylvania*
[2] *Physics & Astronomy Department, New York University Abu Dhabi, Abu Dhabi*

Abstract

The study of exoplanetary atmospheres has opened the door to understanding the diversity of planetary systems other than our own. Transmission and emission spectroscopy have already revealed molecular features that, for example, can indicate the presence of water or point to a hot, uninhabitable world. Analyzing these spectra to reach such conclusions requires atmospheric models that apply radiative transfer theory to generate synthetic spectra, which are then fit to the data. Pyrat-Bay is one such code that uses a Markov Chain Monte Carlo sampler to explore the model parameter space and find the best fit to the observations. Prior to this paper, Pyrat-Bay's forward model did not account for clouds, though several exoplanets have already been found to have clouds obscuring their atmosphere. Here, we present the implementation of a cloud model in Pyrat-Bay. We parametrize the cloud shape and vertical extent and describe how we determine the cloud's base pressure. A particle size distribution for each cloud layer is applied and Mie extinction cross sections are calculated using a pre-interpolated grid of absorption and scattering efficiencies. We demonstrate our working cloud model by running Pyrat-Bay's forward model for different cloud parameters on model atmospheres of HD209458b and Earth. Future work includes implementing this cloud parametrization in the retrieval framework of Pyrat-Bay and running it on transmission spectra observations for hot-Jupiters, in addition to running retrievals with gray clouds and the soon-to-be implemented patchy clouds.

1 Introduction

The quality of the spectra of exoplanetary atmospheres is quickly improving. As a result, we are demanding better models to understand our observations of the physical and chemical signatures of these systems. With the upcoming launch of the James Webb Space Telescope (JWST), we will need to continue improving our models to correctly interpret the spectral signatures in the data. We see much diversity and complexity in the atmospheres of our own solar system planets, and we can expect even more with the hot Jupiters for which we are gathering data.

We have already observed planets whose spectra range from being featureless to ones showing Rayleigh slopes and absorption due to the presence of various molecular species [Heng, 2016, Parmentier et al., 2016, Sing et al., 2016]. For these featureless spectra, it is expected that clouds and hazes are obscuring the atmosphere [Deming et al., 2013, Kreidberg et al., 2014, Sing et al., 2015]. Because the presence of clouds is degenerate with lower molecular abundances, clouds can make analyzing the atmosphere difficult, and ignoring them can cause misleading results. Additionally, clouds influence a planet's habitability by altering the planet's albedo or exhibiting a greenhouse effect. Studying the degree of cloudiness for planets in different environments can lead to interesting implications for planetary formation and evolution theories [Heng, 2016, Heng and Demory, 2013]. The motivation therefore exists for the proper treatment of clouds in exoplanet spectral analysis codes.

Several codes for retrieval of exoplanet atmospheric parameters exist including CHIMERA [Line et al., 2013], NEMESIS [Barstow et al., 2015, Irwin et al., 2008], SCARLET [Benneke, 2015], and BART [Blecic, 2016], to name a few. Of these, only SCARLET includes clouds that are not

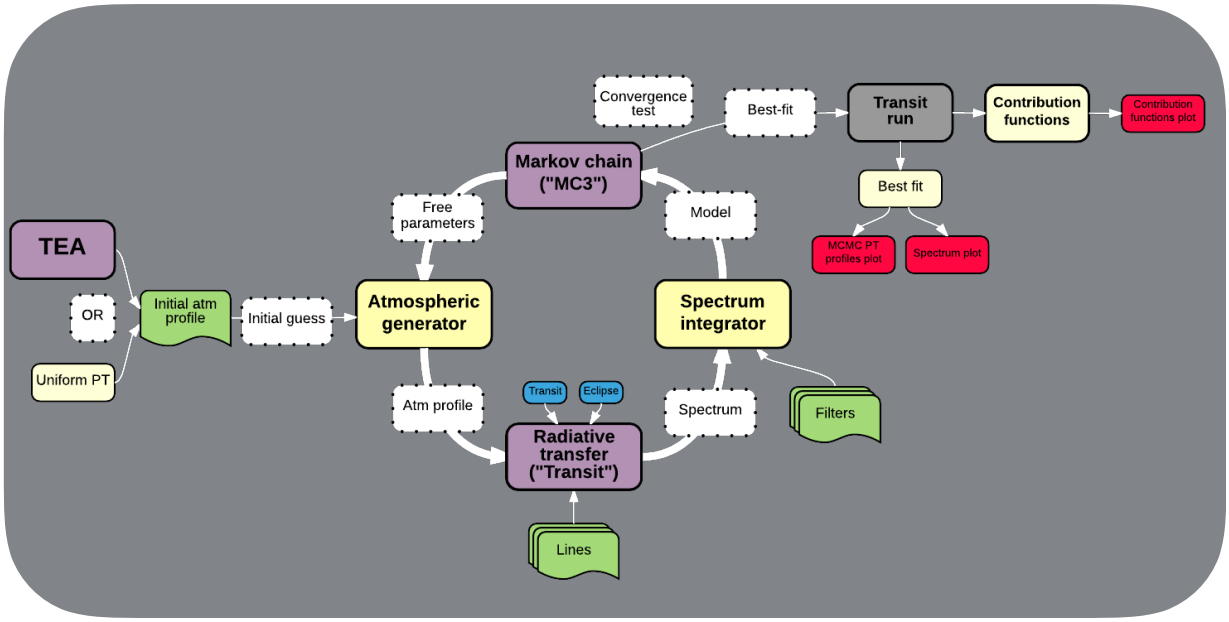

Figure 1: Diagram of BART, the predecessor of Pyrat-Bay. This cloud parametrization was added to the forward model labeled here as 'Transit'.

gray-scatterers. Because clouds truly absorb and scatter light according to Mie theory, the affect cloud particles have on the resultant spectrum that can be much different from that of a gray cloud. Additionally, given certain model atmospheric temperatures and abundances, clouds may not form and thus including them would be physically inconsistent. Patchy clouds, which are notably present on Earth, are also typically ignored by retrieval models because codes designed for studying exoplanet atmospheres are typically one dimensional. It is important, however, to understand the consequences of assuming simplified cloud models in our retrievals.

We address this concern in this paper by first modifying an atmospheric forward model to include a self-consistent cloud parametrization. Then, in future work, we plan to use this tool in its retrieval framework to study the affects of assuming different cloud models when fitting hot Jupiter transmission and emission spectra.

1.1 Pyrat-Bay

The code modified for this project is the Python Radiative Atmospheric Transfer using Bayesian inference (Pyrat-Bay) [Cubillos et al., 2017], which is the successor of BART (Bayesian Atmospheric Radiative Transfer) [Blecic, 2016]. The code is primarily written in Python with several C extensions. The code is well documented and easy to edit, and while it is currently still proprietary, Pyrat-Bay will be made open source in 2017. Pyrat-Bay consists of several components including the Thermal Equilibrium Abundance (TEA) code [Blecic, 2016] and Multi-Core Markov-Chain Monte Carlo (MC3) [Cubillos, 2016], which are both available for download on their own. The forward model includes the radiative transfer physics, which calculates the absorption efficiency for each wavelength at each layer in the atmosphere. Pyrat-Bay is currently set up for both transit and eclipse geometries, however, in this work, we only test our cloud model in the transit geometry mode.

Pyrat-Bay already implements options for either a uniform gray cloud model or one of two different Rayleigh scattering options taken from Dalgarno and Williams [1962] and Lecavelier Des Etangs et al. [2008b], respectively. In this work we add a parameterized cloud to the radiative

transfer forward model in order to more realistically capture the wavelength dependent effect of clouds on transmission and emission spectra and to produce a more self-consistent atmospheric model.

In Section 2, we first discuss typical cloud scale heights and properties in solar system objects. In Section 3, we discuss our cloud parametrization, covering how we define the cloud base and top pressures, the condensate molar fraction at each layer in the cloud, and the corresponding cloud particle size distribution. We use the particle size distribution at each layer in the atmosphere to determine the total absorption and scattering due to Mie theory, which is addressed in Section 3.4. Finally in Section 4, we demonstrate our working cloud model by running Pyrat-Bay's forward model under various assumptions of the cloud parameters. We conclude in Section 5 and discuss our plans for future work on this project.

2 Solar System Planets

To place some context for modeling clouds in exoplanet atmospheres, we first consider the case of planets and moons in our solar system. Clouds are ubiquitous on planets in our solar system that have atmospheres. The diverse set of these clouds depend on the atmospheric height, temperature and pressure profile, and composition of these atmospheres. While Pyrat-Bay is intended for hot-Jupiters, which have much hotter and denser environments than our familiar solar system planets, the same general principles of cloud formation still apply.

For solar system planets, we calculate the approximate cloud scale heights as derived in Sánchez-Lavega A. [2004], that depend on the specific vapor constant, R_V, the temperature at the base of the cloud, T_{cl}, the specific heat capacity, c_p, surface gravity, g, and latent heat, L:

$$H_{cloud} = \frac{R_V T_{cl}^2 c_p}{gL} \tag{1}$$

The scale height of the atmosphere where the cloud forms is $H = \frac{R^* T_{cl}}{g}$, where R^* is the specific gas constant. We determine the cloud base height by finding the intersection of the saturation vapor pressure curve and temperature-pressure profile (see Section 3.1 for a more detailed description of determining cloud base pressure). For the temperature pressure profiles of all solar system planets except Mars, we consolidate probed measurements from Robinson and Catling [2014] with analytic calculations using an expression for a dry adiabatic profile:

$$P(T) = P_0 \Big(\frac{T}{T_0}\Big)^{g/\Gamma_a R^*}. \tag{2}$$

We use the values presented in Sánchez-Lavega A. [2004] for reference pressure, P_0, temperature, T_0, surface gravity, g, and Γ_a, the adiabatic gradient. For Mars, we use a temperature-pressure profile generated using the NASA-Ames Mars General Circulation Model.

For each planet and each condensate species, we plot the cloud scale heights and atmospheric scale heights in Figure 2 as the dark and light shaded regions, respectively. Because atmospheric extent varies for each planet, we can use the ratio of the cloud scale heights to the atmospheric scale heights for each planet as a metric for comparison. Typical values for this ratio range from 10% - 20%.

It is interesting to note the variety of cloud properties in our own solar system alone. Depending on the chemistry and atmospheric conditions, clouds of many different species can form either very close to the surface as in the case of Titan, or at various levels higher in the atmosphere, as seen in the ice and gas giants. A cloud parametrization used in fitting the spectra of exoplanet

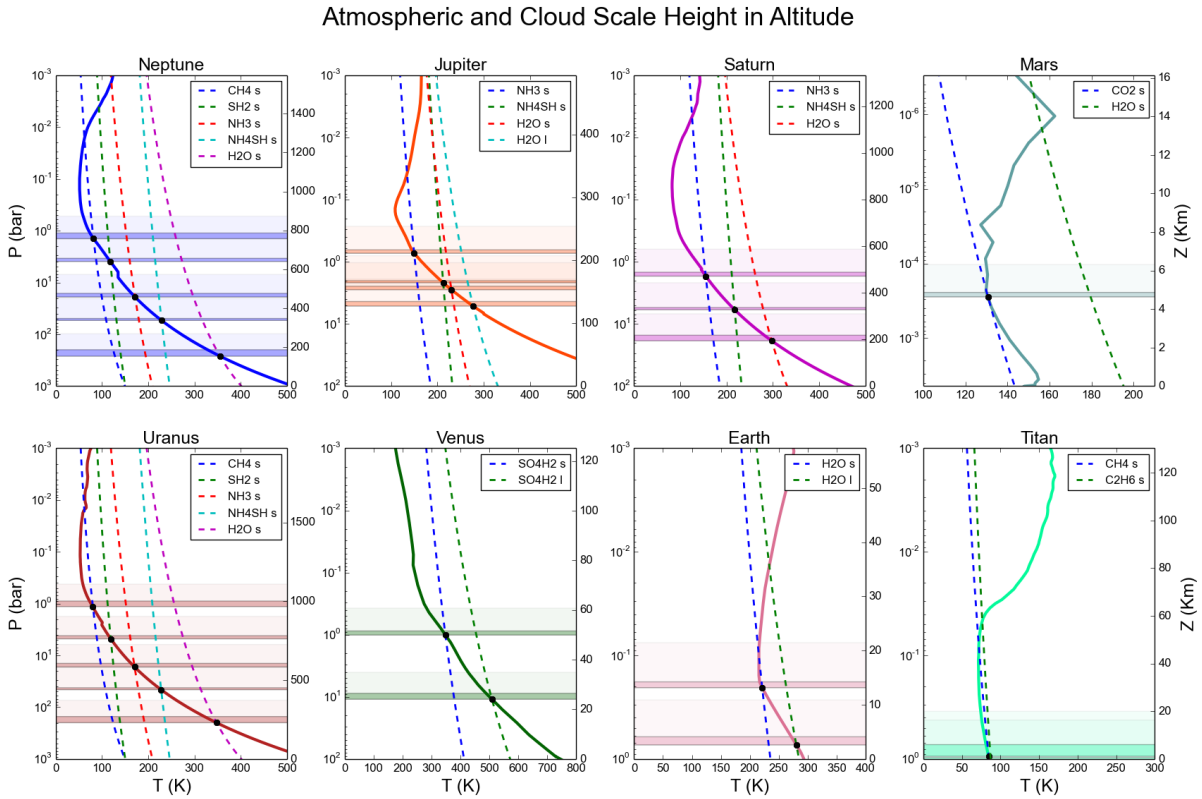

Figure 2: Temperature pressure profiles, saturation pressure curves, and cloud scale heights for Solar System planets. We extend temperature pressure profile data from Robinson and Catling [2014] to deeper pressures using Equation 2 from the text that describes a dry adiabatic pressure profile. The dashed saturation pressure curves are determined using Equation 7. For both calculations, parameters are taken from those listed in Sánchez-Lavega A. [2004]. The cloud scale height is calculated using Equation 1 and shown here as the darker shaded bands. The lighter shaded region represents the scale height of the atmospheres.

atmospheres must allow for at least as much diversity as we see here for solar system planets. For hot-Jupiters, the main difference is the extreme temperatures, which means elements and molecules that we would not normally expect to evaporate on Earth, can now mix into the atmosphere and form clouds. The most commonly considered condensates for hot Jupiter atmospheres are iron and enstatite ($MgSiO_3$).

3 Cloud Parametrization

The parametrization we introduce in this report utilizes Mie theory to produce the realistic extinction effects of clouds. In the following subsections, we go through the steps of defining our parametrized cloud given several cloud-specific free parameters in combination with atmospheric properties defined in Pyrat-Bay. Once the cloud's location and extent in the model atmosphere is determined, we discuss the process of assigning a particle size distribution for cloud droplets at each cloud layer, which we use to determine the Mie scattering extinction as a function of wavelength.

3.1 Cloud Base

In order for clouds of a particular species to form, the vapor pressure of that species must exceed the saturation pressure. The saturation pressure for a particular species is governed by the

Clausius-Clapeyron equation, which describes the slope of the pressure-temperature relationship to temperature, T (Kelvin), given the latent heat of the phase transition, L (J/g), and the specific volume, $V_i = 1/\rho_i$:

$$\frac{dP_V}{dT} = \frac{L}{T(V_2 - V_1)} \tag{3}$$

This relationship can be simplified by assuming the gas phase volume is much larger than the liquid or solid phase volume of the species. Combining this simplification with the ideal gas law allows us to make the substitution $V_2 - V_1 \approx 1/\rho_V \approx R_V T/P$, where we use the subscript V for parameters corresponding to the vapor phase. Before integrating Equation 3, we can redefine the latent heat in terms of the heat capacity, c_p:

$$\Big(\frac{dL}{dT}\Big)_P = \Delta c_p \tag{4}$$

Expanding the heat capacity to second order in temperature with expansion coefficients α and β and integrating once to get latent heat as a function of temperature gives:

$$L = L_0 + \Delta\alpha T + \frac{\Delta\beta}{2}T^2 + O(T^3) \tag{5}$$

Plugging the simplification and expansion into the Clausius-Clapeyron equation and integrating gives us the saturation pressure as a function of temperature:

$$P_V(T) = \exp\Big(\ln C + \frac{1}{R_V}\Big[-\frac{L_0}{T} + \Delta\alpha \ln T + \frac{\Delta\beta}{2}T + O(T^2)\Big]\Big) \tag{6}$$

Because the pressure of the atmosphere is the sum of partial pressures of all the various species, Equation 6 must be divided by the mixing ratio of that species, following from $P_p = X_C P(T) \geq P_V(T)$, where P_p is the partial pressure of the vapor, X_C is the condensate molar mixing ratio, and $P(T)$ just represents the vertical pressure of the atmosphere. The species condenses to form clouds where the partial pressure is greater than the saturation vapor pressure for that species:

$$P(T) = \frac{1}{X_C}\exp\Big(\ln C + \frac{1}{R_V}\Big[-\frac{L_0}{T} + \Delta\alpha \ln T + \frac{\Delta\beta}{2}T + O(T^2)\Big]\Big) \tag{7}$$

Equation 7 is a useful form for defining the pressure at which a species will condense given temperature and the molecular constants for the condensing species. We use Equation 7 to define where clouds form in our model atmospheres.

In practice, we evaluate Equation 7 on the same temperature grid for each atmospheric layer already defined in Pyrat-Bay. Then we choose the cloud base to lie in the layer which has the minimum absolute difference between atmospheric pressure and condensate saturation pressure.

Note that changes in the mixing ratio of the condensate species, X_C, will ultimately shift the pressure of the base of the cloud, which can dramatically change the resultant spectrum. For example, underestimating the molar mixing ratio of a condensing species can lead to higher clouds, which can completely flatten the spectral features in a transmission spectrum if the cloud is thick enough. On the other end, overestimating X_C could lead to no clouds at all because the species only exists in solid form on the planet's surface. One possibility to combat this effect is to allow X_C to be a free parameter and let the data lead to its value in the retrieval process. This is not entirely self-consistent however, because the molar mixing ratio is elsewhere defined at each atmospheric layer in the forward model for each species the user decides to include in the model. This alternate value is input into the code from TEA, which applies thermal equilibrium chemistry

to determine the abundances at each layer. These abundances are allowed to vary slightly in the retrieval process, but not to the extent at which would allow much movement in the position of the cloud base. While the application of thermal equilibrium chemistry to hot Jupiter atmospheres is certainly valid, there is still large uncertainty in our initial assumptions about these atmospheres that propagates to uncertainties in these abundances. We therefore have two options when running retrieval to fit the data: (1) self-consistently define X_C based on the TEA abundances, or (2) allow X_C to be a free parameter, separately defined from TEA-defined abundances. Currently both options are implemented and we plan to run retrieval separately for each method. If in the second option, X_C and the corresponding TEA defined abundance are inconsistent, this could be possibly a result of degeneracies, incorrect abundances due to user defined species inputs, or the need for the consideration of disequilibrium chemistry.

3.2 Condensate Fraction Profile

With the cloud base pressure set, we can next define the vertical extent of the cloud and the condensate fraction at each cloud layer. For this, we adopt a similar parametrization to the one introduced in Benneke [2015] that can reproduce the vertical profile of several other cloud models:

$$q_c(p) = q_*(\log p - \log p_{base})^{H_c}, \quad for \quad p_{top} \leq p \leq p_{base} \tag{8}$$

This equation defines the condensate mole fraction, $q_c \equiv n_C/n_{H_2}$, at pressure p in the cloud layers ranging from the base pressure, p_{base}, to the pressure at the top of the cloud, p_{top}. Here, q_c is the condensate mole fraction at the pressure, p, in the cloud layer. The parameter q_* is the condensate mole fraction one scale height below p_{top} and H_c determines the shape of the cloud profile. We use n_C and n_{H_2} to be the number densities of condensates and H_2 molecules, respectively. Figure 3 is a remake of Figure 2 from Benneke [2015] and plots Equation 8 for various values of H_c and q_*.

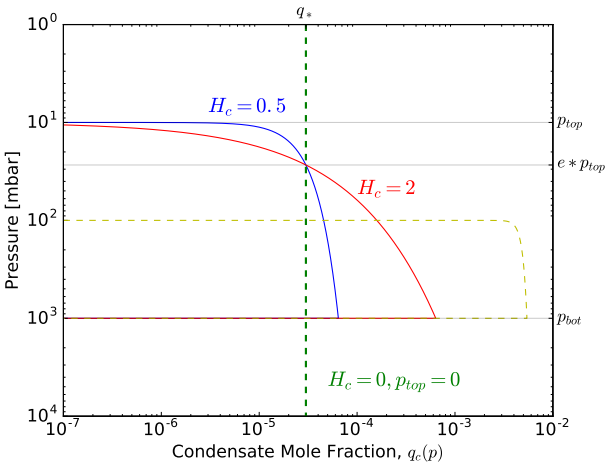

Figure 3: Remake of Benneke [2015]'s Figure 2. Each curve shows condensate mole fraction derived using Equation 8 for various values of H_c and q_*. With p_{bot}, p_{top}, and H_c both equal to zero, we can create a uniform condensate mole fraction throughout the atmosphere as in Lecavelier Des Etangs et al. [2008a]. The red and blue curves recreate similar cloud shapes to those from Ackerman and Marley [2001]. Lowering H_c creates a much steeper cloud deck.

For this parametrization of cloud shape, the code is structured so that q_*, p_{top}, and H_c are free parameters. Increasing q_* by an order of magnitude will noticeably impact the final absorption spectrum, depending on the cloud's vertical height within the atmosphere. Increasing p_{top} would also leave a flatter spectrum by producing a taller cloud that would obscure a larger part of the photosphere. Additionally, p_{base} is determined by X_C, which can also can be allowed to vary. Changing H_c within reasonable limits does not largely affect resultant spectra. Therefore, our initial tests focus on varying q_*, X_C, and p_{top}. See Figures 6 and 7 for how changes in X_C, p_{top} and q_* affect the resultant transmission spectra.

In practice, we define $q_{c,i} = q_c(p_i)$, where p_i are pressure values on the prescribed Pyrat-Bay atmospheric pressure grid. Because the cloud base is also defined on this pressure grid, we can easily define the cloud top pressure using a free parameter we call $i_{\Delta p}$, which is the number of indices in the pressure grid from p_{base} to p_{top}. This simplifies the code and does not compromise the parametrization since the default number of atmospheric layers, $n_{layer} = 100$, allows for more than enough resolution to explore the parameter space.

3.3 Cloud Particle Sizes

At each cloud layer, we have defined q_c according to Equation 8, which is the fraction of condensates based on the number density of H_2. We must now determine the sizes of the cloud particles. In one cloud particle, which we will also refer to here as a droplet, there will be thousands of molecules of that species condensed over an aerosol nucleus. Without the aerosol, the surface tension of the droplet would be too high to form. The microphysics that occurs to go from condensate molecules to a cloud droplet is typically ignored in simpler cloud models since these processes are not well understood to begin with and it is more practical and accurate to assign a particle size distribution based on actual measurements of cloud particle sizes. We therefore ignore this microphysics as well and follow the methods of Ackerman and Marley [2001] of assuming a lognormal distribution for our cloud particle sizes, defined as:

$$n(r) \propto \frac{1}{r\sqrt{2\pi}\ln\sigma_g} \exp\Big[-\frac{\ln^2(r/r_g)}{2\ln^2\sigma_g}\Big], \tag{9}$$

where σ_g is the geometric standard deviation and r_g is the geometric mean radius. This distribution requires a normalization constant, N, which should be determined such that the integral of the distribution is equal to the total number of cloud particles. This is also linked to the condensate mole fraction, q_c, since many of these individual particles bond to create a larger cloud droplet.

To calculate N, we sum over the number of molecules per cloud droplet for each radius bin and set that equal to $q_c n_{H_2}$, the total number of molecules that must condense at that cloud layer. The number of molecules per cloud droplet can be estimated by taking the volume ratio of a cloud droplet to a molecule. Because the cloud droplet core is an aerosol, we must take the effective volume of the outer shell that is actually composed of condensate molecules. We estimate this by always assuming the aerosol radius is 80% of the total radius of the droplet. This propagates to a constant reduced factor in effective droplet size to 50% of the volume of the cloud droplet, $V_{droplet}$. This assumption is not well justified and a better method may be to assume that the core condensation nuclei (CCN) follows a distribution of center $\sim 0.2\mu m$ as found in Broekhuizen et al. [2006]. In either case, an error in either of these methods propagates to having too few or too many cloud particles. Since the magnitude of this offset is small and is degenerate with q_c, which is variable based on our free parameters, we do not worry about this subtlety. Overall this summarizes to finding N satisfying the following:

$$N \sum_i n_i dr_i \frac{0.5 V_{droplet,i}}{V_C} = q_C n_{H_2}, \tag{10}$$

where we use V_C to denote the volume of the condensate molecule and i refers to the index of a radius bin. Figure 4 shows an example distribution with σ_g set to 1.8, which we do for all runs. This reduces the number of free parameters for retrieval and reasonable changes to the width of the particle size distribution do not strongly affect the resultant cloud absorption. We construct the code such that r_g can be a free parameter, however we do not vary it for runs in this paper and

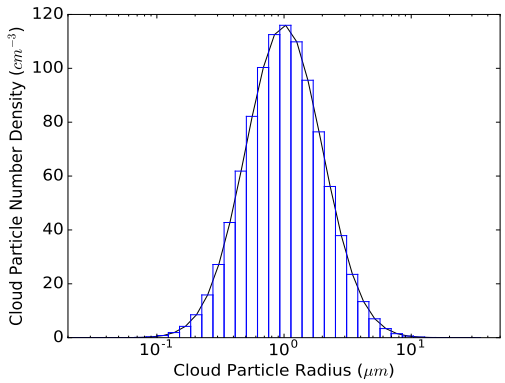

Figure 4: Example particle size distribution for cloud particles. In blue we show the distribution binned into the default of 40 radii bins. The distribution is normalized such that the sum over radius bins gives the total number of condensates.

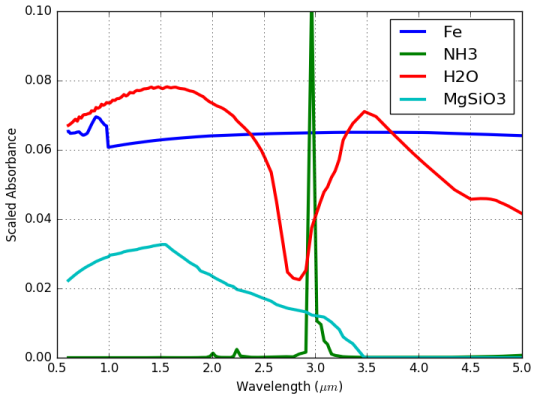

Figure 5: Absorbance shapes for one atmospheric layer for Fe, $MgSiO_3$, NH_3, and H_2O. All clouds are arbitrarily scaled to be visible within the same limits, assuming a mean of $10\mu m$ for the particle size distribution.

instead leave it to be $10\mu m$. For simplicity, we currently define the same distribution at each layer of the cloud, but we normalize it based on the condensate fraction, q_c, defined for that layer.

3.4 Scattering & Absorption

For the wavelengths under consideration, our cloud particle sizes are large enough to require Mie theory to describe the particles' interaction with light. We utilize the code used by Ackerman and Marley [2001] to calculate absorption and scattering efficiencies for the condensate species we consider. Their code is adapted from Toon and Ackerman [1981], which modified the code of Dave [1969] that computes scattering of electromagnetic radiation by a sphere. Toon and Ackerman [1981] adapted the code for a stratified sphere, which is applicable to the case of a cloud particle containing an aerosol center surrounded by a shell of the condensate.

The Mie scattering code takes inputs of real and imaginary refractory indices for a particular species and calculates Q_a and Q_s, which are the absorption and scattering efficiencies, respectively, as a function of wavelength and particle radius. For this work, we use the Ackerman and Marley [2001] Mie extinction code to generate Q_a and Q_s and then perform a 2D interpolation of these coefficients over wavelength and cloud droplet radius. These efficiencies are related to what we call absorbance per layer, $A_q(\lambda)$, in units of inverse centimeters, by the following equations:

$$C_e(\lambda, r) = Q_a \pi r^2 + Q_s \pi r^2, \tag{11}$$

$$A_q(\lambda) = \sum_r n(r) C_e(\lambda, r). \tag{12}$$

Here, C_e is the extinction cross section, $n(r)$ is the droplet number density defined by Equation 9, and each layer of the cloud is indexed by q. Multiplying the A_q by the thickness of the cloud layer gives the optical depth for that layer. Example absorbance spectra for water, iron, enstatite, and ammonia are shown in Figure 5. A gray cloud would be a horizontal line on this plot.

The values of $A_q(\lambda)$ for each species are summed up and returned to Pyrat-Bay's optical depth class for the radiative transfer calculation.

4 Results

Here we demonstrate the cloud parametrization implemented in the Pyrat-Bay forward model. We run the forward model for Earth and for the hot Jupiter HD209458b using its temperature-pressure profile taken from Line et al. [2014] and acquiring abundances of molecules at each atmospheric layer using TEA. We note that thermal equilibrium chemistry makes assumptions that do not hold for Earth and that new analysis suggests that the temperature-pressure profile of HD209458b has no thermal inversion [Line et al., 2016]. We emphasize, however, that these applications of the code are solely for demonstration purposes and so for these specific tests we are not concerned with modeling these particular test planets with complete accuracy.

4.1 HD209458b

The transiting planet HD209458b is a hot Jupiter orbiting a G dwarf with a period of 3.5 days and is approximately 30% less massive than Jupiter [Wang and Ford, 2011]. HD209458b is a very well studied hot Jupiter with transmission spectra and thermal emission measurements [Schwarz et al., 2015, Sing et al., 2008, Snellen et al., 2008] making it a good test subject for future retrieval. We include line absorption profiles of CO_2, CO, CH_4, and H_2O for the radiative transfer calculation taken from the HITRAN database. In addition to these, eleven other molecules relevant to hot Jupiters are present in the model atmosphere including hydrocarbons, ammonia, and iron.

We run the Pyrat-Bay forward model assuming the planet properties of HD209458b and a cloud composed of iron and show the results for a range of cloud parameters in Figure 6. For all runs, we set H_c to 1.0 and r_g to $10\mu m$. In panel (a) of Figure 6 we vary the cloud top pressure and set $X_C = 10^{-9}$ and $q_* = 10^{-4}$. As the cloud extent increases, a larger portion of the atmosphere becomes opaque and photons no longer pass below the cloud layer. As a result, the planet appears larger in radius in that wavelength region. While the cloud with the largest vertical extent really washes out all the spectral features, it is important to note that in this atmosphere, the iron cloud is unphysical since the cloud extends past the point where the saturation vapor pressure curve begins to exceed the temperature-pressure profile because of the temperature inversion. Of course high altitude clouds are possible when there is no thermal inversion, but in cases where clouds are only present deeper in the atmosphere, the upper portion of the atmosphere will be left unobscured.

In Figure 6b, we vary q_*, which controls the number of cloud particles present in the cloud layers. For these runs, we exaggerate the pressure extent of the clouds so that the results become more pronounced. The cloud extent indicated in the temperature-pressure profile corresponds to an $i_{\Delta p} = 20$, out of 100 atmospheric layers. We also set X_C to 10^{-9}. As expected, increasing the number of condensates increases the opacity resulting in fewer photons passing through the layers of the atmosphere below the cloud. After a certain particle density, increasing the density does not affect the result because cloud has become effectively opaque over all wavelengths.

The effects of changing X_C are shown in Figure 6c. For these runs, q_* was set to 10^{-4} and the pressure extent corresponds to $i_{\Delta p} = 10$. By changing the mixing ratio of condensates, we lower the point in the atmosphere at which saturation will be reached and clouds will form. The higher the cloud, the larger the fraction of atmosphere that is opaque.

4.2 Earth

A similar process was done for Earth using the temperature-pressure profile from Figure 2. For molecular absorption we include line lists for H_2O from the HITRAN database. The model atmosphere also contains carbon, nitrogen, oxygen, and hydrogen and eight molecules common to

Earth's atmosphere composed of those four elements. The results for introducing a liquid water cloud with various values for q_*, X_C, and $i_{\Delta p}$ are shown in Figure 7.

It is clear from these plots that there are many degeneracies between the cloud parameters. Running retrieval will reveal the parameter correlations. These degeneracies will somewhat be reduced in running retrieval on observations with appropriate prior distributions. In particular, constraints on the cloud extent can be made to ensure the clouds are physical. By requiring X_C to match the abundances defined for that species according to equilibrium chemistry and user assumptions about the atmospheric chemistry, this parameter can be eliminated leaving a more self-consistent atmospheric model. Since the environments of hot Jupiters and their atmospheric chemistry are not well understood, microphysical cloud models and experiments that study the range of physical possibilities of cloud formation will also be very helpful in eliminating unphysical conclusions. Overall, it is important to allow the data guide the parameters to their best fit values in order to understand the parameter correlations and uncertainties. However, because of the large number of parameters possible, making reasonable assumptions becomes necessary to reduce the number of free parameters to some degree, especially if including multiple clouds of different species.

5 Conclusions & Future Work

In summary, we have implemented a realistic, parametrized cloud model in the soon-to-be open source Pyrat-Bay retrieval code. This model is described by five parameters for each condensate species, though it is reasonable to keep fixed the mean of the lognormal particle size distribution, r_g, and the cloud shape factor, H_c, because they do not strongly influence the resulting transmission spectrum. In future work, we plan to run retrieval using this upgraded version of Pyrat-Bay on transmission spectra for a few hot Jupiters in order to understand the degeneracies amongst the cloud parameters, to assess the improvements clouds have on the fit, and to study the effects that adding clouds has on the rest of the model parameters.

Gray clouds are already implemented in Pyrat-Bay. The gray cloud model parameters are a constant cross section and base and top pressures that define the extent of the cloud. In future work we plan on implementing a patchy cloud option that defines the fraction of cloud coverage. With a gray cloud model, a patchy cloud parameter, and the Mie scattering cloud model implemented in this work, we will be able to run retrievals with each different model on data of HD189733b, HD209458b, and other hot Jupiters and answer questions such as which model performs best for each planet, what degeneracies exist amongst model parameters, and to what extent we can constrain cloud content on these planets.

In future work we also wish to deduce how well we will be able to answer similar questions provided with data from the James Webb Space Telescope (JWST). With JWST passbands and noise models, we can anticipate how our constraints on exoplanet atmospheres will improve with advanced JWST technology.

6 Acknowledgements

We would like to thank the Kavli Summer Program in Astrophysics for the fun and extremely beneficial experience that made this work possible. This includes the Kavli Institute for their generous support of the program and Pascale Garaud, Jonathan Fortney and the rest of the organizing committee that ensured the program was a success in every way. We would also like to thank program participants Ty Robinson and David Catling for the temperature-pressure profiles of solar

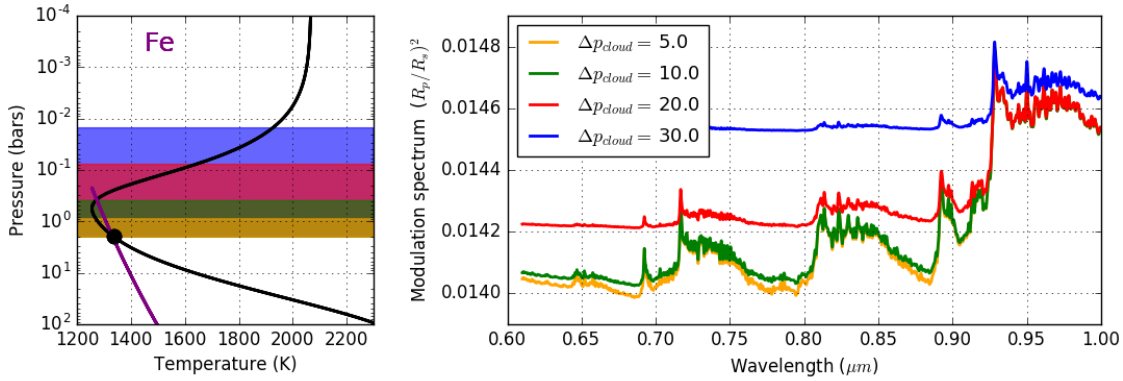

(a) Changing the cloud top pressure, keeping all else fixed.

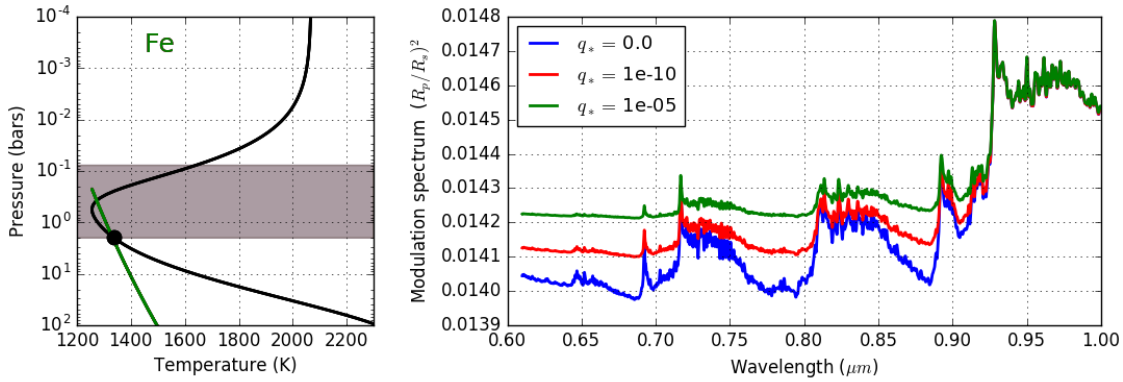

(b) Changing q_* keeping cloud position and shape fixed.

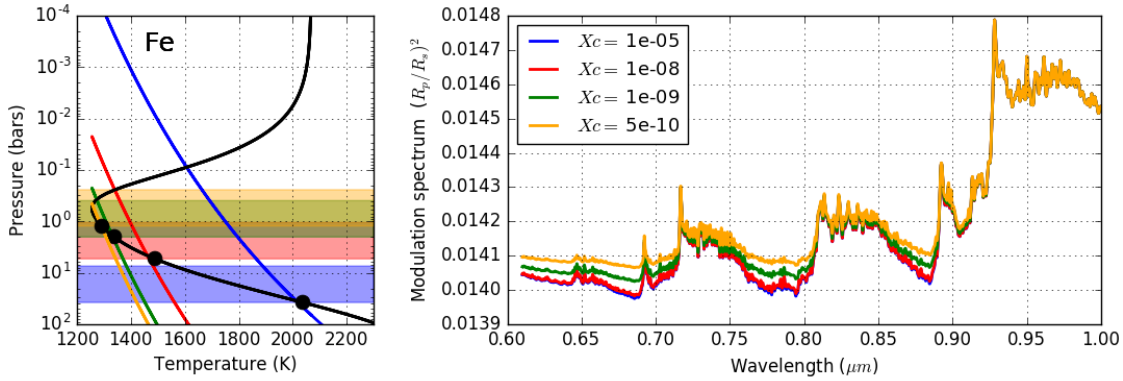

(c) Changing the mixing ratio of the condensate species.

Figure 6: **Left**: Temperature-pressure profiles of HD209458b. Vapor pressure curves shown are for iron. Iron clouds would form at the intersection marked by a black point. Apparent offsets are due to defining the cloud base on Pyrat-Bay's predetermined atmospheric pressure grid. **Right**: Transmission spectra of HD209458b including line absorption profiles of CO_2, CO, CH_4, and H_2O. Increasing q_*, decreasing X_C, and increasing Δp all flatten the spectrum of HD209458b. See text for more information.

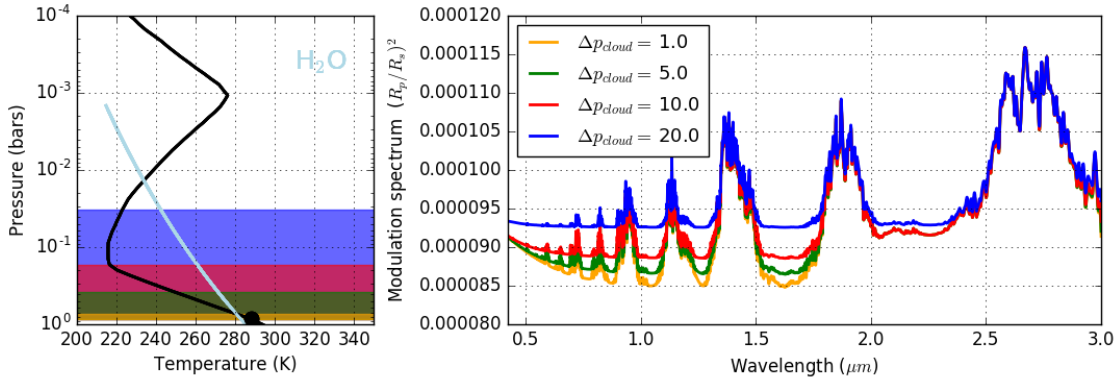

(a) Changing the cloud top pressure, keeping all else fixed.

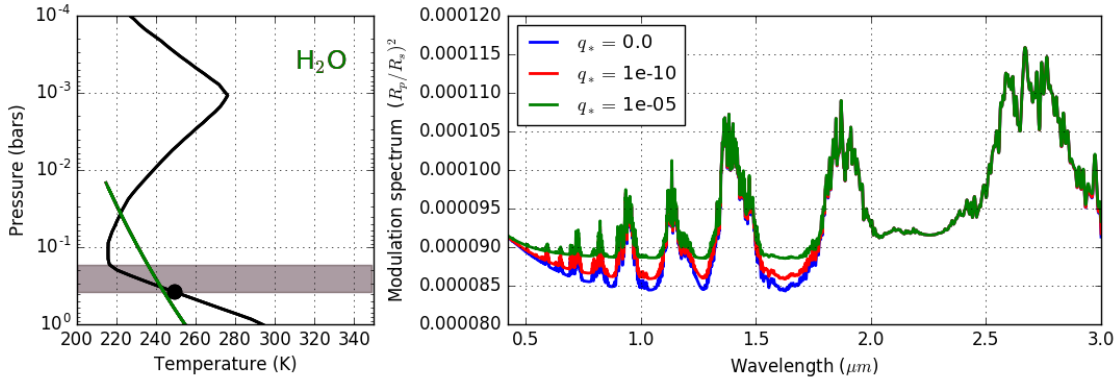

(b) Changing q_* keeping cloud position and shape fixed.

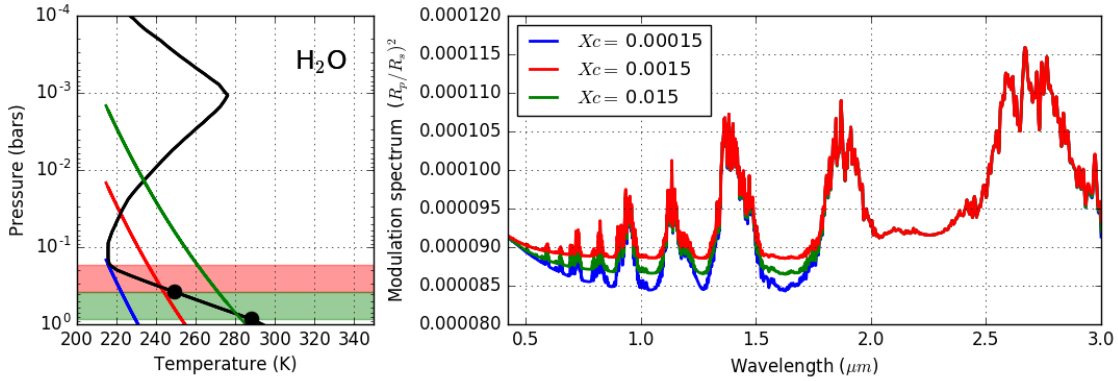

(c) Changing the mixing ratio of the condensate species.

Figure 7: **Left**: Temperature-pressure profiles of Earth. Vapor pressure curves shown are for liquid water. Water clouds would form at the intersection marked by a black point. Apparent offsets are due to defining the cloud base on Pyrat-Bay's predetermined atmospheric pressure grid. **Right**: Transmission spectra of Earth including line absorption profiles of H_2O. Increasing q_*, decreasing X_C, and increasing Δp all flatten the spectrum of Earth. See text for more information.

system planets and Cecilia Leung for generating the temperature profile of Mars using the NASA Ames Mars GCM.

References

A. S. Ackerman and M. S. Marley. Precipitating Condensation Clouds in Substellar Atmospheres. , 556:872–884, August 2001. doi: 10.1086/321540.

J. K. Barstow, N. E. Bowles, S. Aigrain, L. N. Fletcher, P. G. J. Irwin, R. Varley, and E. Pascale. Exoplanet atmospheres with EChO: spectral retrievals using EChOSim. *Experimental Astronomy*, 40:545–561, December 2015. doi: 10.1007/s10686-014-9397-y.

B. Benneke. Strict Upper Limits on the Carbon-to-Oxygen Ratios of Eight Hot Jupiters from Self-Consistent Atmospheric Retrieval. *ArXiv e-prints*, April 2015.

J. Blecic. Observations, Thermochemical Calculations, and Modeling of Exoplanetary Atmospheres. *ArXiv e-prints*, April 2016.

K Broekhuizen, RY-W Chang, WR Leaitch, S-M Li, and JPD Abbatt. Closure between measured and modeled cloud condensation nuclei (ccn) using size-resolved aerosol compositions in downtown toronto. *Atmospheric Chemistry and Physics*, 6(9):2513–2524, 2006.

P. Cubillos, J. Blecic, and J. Harrington. Python Radiative Atmospheric Transfer using Bayesian inference. 2017.

P. E. Cubillos. Characterizing Exoplanet Atmospheres: From Light-curve Observations to Radiative-transfer Modeling. *ArXiv e-prints*, April 2016.

A. Dalgarno and D. A. Williams. Rayleigh Scattering by Molecular Hydrogen. , 136:690–692, September 1962. doi: 10.1086/147428.

J. V. Dave. Scattering of electromagnetic radiation by a large, absorbing sphere. *IBM J. Res. Dev.*, 13(3):302–313, May 1969. ISSN 0018-8646. doi: 10.1147/rd.133.0302. URL `http://dx.doi.org/10.1147/rd.133.0302`.

D. Deming, A. Wilkins, P. McCullough, A. Burrows, J. J. Fortney, E. Agol, I. Dobbs-Dixon, N. Madhusudhan, N. Crouzet, J.-M. Desert, R. L. Gilliland, K. Haynes, H. A. Knutson, M. Line, Z. Magic, A. M. Mandell, S. Ranjan, D. Charbonneau, M. Clampin, S. Seager, and A. P. Showman. Infrared Transmission Spectroscopy of the Exoplanets HD 209458b and XO-1b Using the Wide Field Camera-3 on the Hubble Space Telescope. , 774:95, September 2013. doi: 10.1088/0004-637X/774/2/95.

K. Heng. A Cloudiness Index for Transiting Exoplanets Based on the Sodium and Potassium Lines: Tentative Evidence for Hotter Atmospheres Being Less Cloudy at Visible Wavelengths. , 826: L16, July 2016. doi: 10.3847/2041-8205/826/1/L16.

K. Heng and B.-O. Demory. Understanding Trends Associated with Clouds in Irradiated Exoplanets. , 777:100, November 2013. doi: 10.1088/0004-637X/777/2/100.

P. G. J. Irwin, N. A. Teanby, R. de Kok, L. N. Fletcher, C. J. A. Howett, C. C. C. Tsang, C. F. Wilson, S. B. Calcutt, C. A. Nixon, and P. D. Parrish. The NEMESIS planetary atmosphere radiative transfer and retrieval tool. , 109:1136–1150, April 2008. doi: 10.1016/j.jqsrt.2007.11.006.

L. Kreidberg, J. L. Bean, J.-M. Désert, B. Benneke, D. Deming, K. B. Stevenson, S. Seager, Z. Berta-Thompson, A. Seifahrt, and D. Homeier. Clouds in the atmosphere of the super-Earth exoplanet GJ1214b. , 505:69–72, January 2014. doi: 10.1038/nature12888.

A. Lecavelier Des Etangs, F. Pont, A. Vidal-Madjar, and D. Sing. Rayleigh scattering in the transit spectrum of HD 189733b. , 481:L83–L86, April 2008a. doi: 10.1051/0004-6361:200809388.

A. Lecavelier Des Etangs, A. Vidal-Madjar, J.-M. Désert, and D. Sing. Rayleigh scattering by H_2 in the extrasolar planet HD 209458b. , 485:865–869, July 2008b. doi: 10.1051/0004-6361:200809704.

M. R. Line, H. Knutson, A. S. Wolf, and Y. L. Yung. A Systematic Retrieval Analysis of Secondary Eclipse Spectra. II. A Uniform Analysis of Nine Planets and their C to O Ratios. , 783:70, March 2014. doi: 10.1088/0004-637X/783/2/70.

M. R. Line, K. B. Stevenson, J. Bean, J.-M. Desert, J. J. Fortney, L. Kreidberg, N. Madhusudhan, A. P. Showman, and H. Diamond-Lowe. No Thermal Inversion and a Solar Water Abundance for the Hot Jupiter HD209458b from HST WFC3 Emission Spectroscopy. *ArXiv e-prints*, May 2016.

Michael R. Line, Aaron S. Wolf, Xi Zhang, Heather Knutson, Joshua A. Kammer, Elias Ellison, Pieter Deroo, Dave Crisp, and Yuk L. Yung. A systematic retrieval analysis of secondary eclipse spectra. i. a comparison of atmospheric retrieval techniques. *The Astrophysical Journal*, 775(2): 137, 2013. URL `http://stacks.iop.org/0004-637X/775/i=2/a=137`.

V. Parmentier, J. J. Fortney, A. P. Showman, C. Morley, and M. S. Marley. Transitions in the Cloud Composition of Hot Jupiters. , 828:22, September 2016. doi: 10.3847/0004-637X/828/1/22.

T. D. Robinson and D. C. Catling. Common 0.1bar tropopause in thick atmospheres set by pressure-dependent infrared transparency. *Nature Geoscience*, 7:12–15, January 2014. doi: 10.1038/ngeo2020.

H. Schwarz, M. Brogi, R. de Kok, J. Birkby, and I. Snellen. Evidence against a strong thermal inversion in HD 209458b from high-dispersion spectroscopy. , 576:A111, April 2015. doi: 10.1051/0004-6361/201425170.

D. K. Sing, A. Vidal-Madjar, J.-M. Désert, A. Lecavelier des Etangs, and G. Ballester. Hubble Space Telescope STIS Optical Transit Transmission Spectra of the Hot Jupiter HD 209458b. , 686:658-666, October 2008. doi: 10.1086/590075.

D. K. Sing, H. R. Wakeford, A. P. Showman, N. Nikolov, J. J. Fortney, A. S. Burrows, G. E. Ballester, D. Deming, S. Aigrain, J.-M. Désert, N. P. Gibson, G. W. Henry, H. Knutson, A. Lecavelier des Etangs, F. Pont, A. Vidal-Madjar, M. W. Williamson, and P. A. Wilson. HST hot-Jupiter transmission spectral survey: detection of potassium in WASP-31b along with a cloud deck and Rayleigh scattering. , 446:2428–2443, January 2015. doi: 10.1093/mnras/stu2279.

D. K. Sing, J. J. Fortney, N. Nikolov, H. R. Wakeford, T. Kataria, T. M. Evans, S. Aigrain, G. E. Ballester, A. S. Burrows, D. Deming, J.-M. Désert, N. P. Gibson, G. W. Henry, C. M. Huitson, H. A. Knutson, A. L. D. Etangs, F. Pont, A. P. Showman, A. Vidal-Madjar, M. H. Williamson, and P. A. Wilson. A continuum from clear to cloudy hot-Jupiter exoplanets without primordial water depletion. , 529:59–62, January 2016. doi: 10.1038/nature16068.

I. A. G. Snellen, S. Albrecht, E. J. W. de Mooij, and R. S. Le Poole. Ground-based detection of sodium in the transmission spectrum of exoplanet HD 209458b. , 487:357–362, August 2008. doi: 10.1051/0004-6361:200809762.

Hueso R. Sánchez-Lavega A., Pérez-Hoyos S. Clouds in planetary atmospheres: A useful application of the clausius clapeyron equation. *American Journal of Physics*, 72(6):767–774, 2004. doi: http://dx.doi.org/10.1119/1.1645279. URL `http://scitation.aip.org/content/aapt/journal/ajp/72/6/10.1119/1.1645279`.

Owen B. Toon and T. P. Ackerman. Algorithms for the calculation of scattering by stratified spheres. *Appl. Opt.*, 20(20):3657–3660, Oct 1981. doi: 10.1364/AO.20.003657. URL `http://ao.osa.org/abstract.cfm?URI=ao-20-20-3657`.

Ji Wang and Eric B. Ford. On the eccentricity distribution of short-period single-planet systems. *Monthly Notices of the Royal Astronomical Society*, 418(3):1822–1833, 2011. doi: 10.1111/j.1365-2966.2011.19600.x. URL `http://mnras.oxfordjournals.org/content/418/3/1822.abstract`.